

ABSTRACT

EVOLUTION AND INTERNAL DYNAMICS OF QUASI-STATICALLY SHEARED GRANULAR FLOWS

Jih-Chiang Tsai

Jerry P. Gollub

Granular materials are collections of particles whose sizes range from microns to meters. They can be packed as a static solid pile and can also move like fluid or gas. When driven at a sufficiently low rate under a compressive load, the grains flow in a quasi-static regime, in which they creep while maintaining simultaneous contacts with multiple neighbors.

We investigate experimentally a quasi-static flow of glass beads packed and sheared in an annular channel. The experiments utilize techniques of refractive-index-matched fluorescent imaging, particle tracking, and simultaneous measurements of volume and boundary shear force. Under long-term shearing, a crystallization transition accompanied by a step-wise decrease of packing volume and shear force can occur. This transition also alters the structure of the internal velocity field. Boundary conditions can affect the crystalline ordering throughout the entire packing. We find that, even under identical boundary conditions and shearing, the evolution of the packing can lead to non-unique final states. The behavior in response to shearing is influenced by the past history of the packing.

Our measurements of the internal velocity fields have a dynamical range of five decades; parameters such as packing thickness and particle size are varied systematically. We demonstrate the impact of crystalline ordering on the spatial gradient of grain velocity - a significant change of local rheology occurs as a consequence of the coherent grain motion. Changing particle size does not influence the gradient of particle velocity significantly; the velocity decay length does not show a direct scaling with particle size. In addition, we

make time-resolved measurements of the anomalous mobility of internal grains immediately following the reversal of boundary motion; this transient behavior reflects the adjustment of the anisotropic contact network. We show that about 20 layers are needed to reveal bulk properties of a granular packing, such as the shear banding of velocity field, the development of distinct states of internal order, and the anomalous mobility upon shear reversal. The effects of stationary boundaries on the spatial decay of velocity with distance from the shearing surface are discussed, based on both theoretical analyses and experimental data on several systems.

Contents

Acknowledgements	iv
Abstract	vi
List of Figures	xix
1 Introduction	1
1.1 Slowly creeping granular materials	2
1.2 Scope of the present work	5
1.3 Granular flows in other regimes	6
2 Experimental Methods	8
2.1 Main apparatus	9
2.2 Internal imaging and image analysis	11
3 Crystallization Transition	14
3.1 Characterization of the transition	15
3.2 Role of bottom condition	19
3.3 Timescales of transition and behaviors of packings of different thickness . .	20
3.4 Discussion	23
4 Non-unique Selection of Final States	25
4.1 Stochastic outcomes of unidirectional shearing combined with oscillatory pre-treatment	26
4.2 Shear-induced stabilization of the disordered state	28

4.3	Discussion	28
5	Quasi-static Internal Dynamics	31
5.1	Steady flows	32
5.1.1	Effects of crystalline order	32
5.1.2	Effects of system size and particle size	35
5.1.3	Invariance for changes in driving speeds and normal loads	37
5.1.4	Effective macroscopic friction	37
5.2	Transient response to shear reversals	38
5.2.1	Grain motions during the shear-reversal transient of a thick packing	38
5.2.2	Change of volume in response to shear reversals	41
5.2.3	Development of shear-reversal transient with packing thickness . . .	42
5.3	Discussion	43
5.3.1	Shear banding	43
5.3.2	Characteristic decay length of velocity field	45
5.3.3	Development of bulk properties with packing thickness	47
5.3.4	Rate-independent frictional dynamics	48
5.3.5	Granular flows vs. Fluid flows	49
6	Conclusions	67
A	Theoretical treatments	74
A.1	Criterion on stress and shear rate for creating a quasi-static granular flow .	75
A.2	Velocity fields of ordinary fluid in a rectangular channel	77
A.3	Derivation of Eqn (5.7)	79
B	Supplements	81
B.1	Tracking individual particles	82
B.1.1	Quality of Dark Disk Tracking	82
B.1.2	Statistics on measured individual particle displacements	82
B.2	Precision measurements of velocity fields	85
B.2.1	Local imaging at different frame rates and image calibration	85

B.2.2 Stochastic variation and measurement uncertainties 87

Bibliography **89**

List of Figures

2.1	Cross-section of the annular channel filled with glass beads.	9
3.1	Simultaneous measurement of internal ordering, volume change, shear force, and particle speed, as functions of time.	16
3.2	Sample histories of evolution.	17
3.3	(a) Compaction histories for fluid-immersed grains of different layer thickness; (b) Compaction history of dry grains.	21
3.4	Non-smooth dependence of the final height $h_f(M)$ of the crystallized flows on the total amount (mass M) of glass beads.	22
4.1	Non-unique selection of final states, indicated by the long-term evolution of the packing height $h(t)$	27
5.1	The three-dimensional structure of the velocity fields. (a) Velocity profiles before crystallization; (b) Velocity profiles after crystallization.	54
5.2	Time-resolved particle trajectories sampled at horizontal (xy) internal planes.	55
5.3	Vertical profiles of steady-state velocity for different states of order and with different boundary conditions.	56
5.4	Vertical profiles of the steady-state velocity, measured from packings of different thickness H_0	57
5.5	Vertical profiles of steady-state velocity for particles of different sizes.	58
5.6	Vertical profiles of normalized steady-state mean velocity, driven at different driving speeds.	59
5.7	Vertical profiles of normalized steady-state mean velocity for deep layers, under different normal loads.	60

5.8	The trajectories of centers of individual grains during $12d$ of boundary displacement, at different stages of a shear-reversal experiment: (a) steady shearing in the positive x direction; (b) the first $12d$ of boundary motion in the opposite direction (negative x); (c) the next $12d$ of boundary motion in the negative x direction following (b).	61
5.9	Time-resolved particle velocity sampled at different heights (z) of the flow, as the boundary velocity $U(t)$ is repetitively reversed in steps.	62
5.10	Time-resolved average grain velocity at the mid-height of a 24-layer packing, subject to a fixed protocol of shear reversal but with the driving speed varying by two orders of magnitude.	63
5.11	The response to shear reversal inside a 24-layer packing.....this demonstrates that a total boundary translation of about $12d$ is insufficient for the packing to fully adjust to the new shearing direction.	64
5.12	The horizontal velocity $U(t)$ and vertical displacement $h(t)$ of the upper boundary as the shearing is repetitively reversed.	65
5.13	Development of the shear-reversal transients with the packing thickness H_0 .	66
A.1	Schematic representation of a granular shear flow.	75
A.2	The solution of Laplace equation $\nabla_{yz}^2 \Phi = 0$ with no-slip boundary conditions.	78
B.1	Sample images showing the quality of Dark Disk Tracking.	83
B.2	Statistics of captured vertical displacements of individual particles.	84
B.3	The sampling rates for different local image patches.	86
B.4	Variation and uncertainties in measuring the vertical profile of time-averaged velocity.	88

Chapter 1

Introduction

1.1 Slowly creeping granular materials

Granular materials are noteworthy both for the range of surprising phenomena they exhibit, and for the challenges they provide to theoretical explanation [4, 9, 18, 38]. Granular materials usually mean collections of particles, whose sizes range from microns to meters. They can be packed as a static solid pile, or can be driven to flow like fluid or gas. One extreme case of granular flows is the rapid-flow regime: the dynamics of rapidly colliding particles is often described using the framework of dissipative kinetic theory with flowing grains bearing some resemblance to molecules in a gas. On the other hand, when particles do not have sufficient relative speed to sustain the imposed pressure - either by an externally imposed compression or due to the weight of grains under gravity, these particles tend to collapse into a dense state of slow creeping. This regime of slowly creeping grains is often termed “quasi-static” in the sense that particles are almost always in static equilibrium, supported by direct contacts with multiple neighbors while creeping around each other. In this regime, the inertia of individual grains plays negligible role in the flow dynamics. Slow geological flows [31] provide examples in which grains throughout the entire granular packing are moving in the quasi-static regime. In granular flows that are highly inhomogeneous, quasi-static creeping and rapid flow can often coexist, such as the particles in industrial blenders [33, 39]. In Appendix A.1, we provide a more precise criterion and a dimensionless number to characterize the quasi-static regime.

Quasi-static granular flows can exhibit rich phenomena, such as long-term evolution and dependence on prior history. These complexities are also found in many other glassy or nearly jammed physical systems. A simple feature of granular particles is that they interact with each other via short-range direct contact forces, in contrast to the long range interactions often present for suspended colloids or other complex fluids. Experimentally, monitoring dense granular packings driven by continuous boundary shear is a useful way to study the evolution of quasi-static flows. For instance, an apparently steady state can gradually undergo substantial change or, in some cases, make a stepwise transition as we report in this work.

Experimentalists have investigated quasi-static granular flows from various points of view. Observations by Komatsu et al. [27] on particles in a thick but quasi 2D pile of

flowing sand imply that the velocity of creeping grains can extend far from the surface into the deep bulk, spanning several orders of magnitude. Behringer and co-workers [32] measure the local contact forces at the lower boundary of a slowly sheared dense granular packing: the fluctuation spectrum (with frequencies scaled by the boundary driving velocity) of local contact forces is invariant over a wide range of driving speeds. This observation illustrates the quasi-static nature of the creeping flow, i.e. the grains are almost always in static equilibrium. Mueth et al. [36] use an MRI technique to study particles in a sheared layer several grain diameters thick, and determine the internal mass flow with sub-grain-size spatial resolution. They have pointed out the effect of particle layering on the mass flow field. In addition, the fluctuating motion of granular particles at the bottom of a Couette shear cell [35], or at its upper surface [5], has been measured; the relation between the local velocity gradient and the fluctuating components of grain motion has been studied in depth. More recently, an experimental study of slowly driven granular flows using a Couette geometry modified with a split bottom [16] shows that the location of the *shear band* (the locus of local maximum of velocity gradient) is determined by the global geometry of a shear cell, while the width of the shear band can be influenced by the properties of the grains such as their size.

To develop understanding beyond a steady-state description of granular flows, it is important to observe time-dependent behaviors. For instance, it is found that when the amplitude of an uniformly imposed cyclic shearing is changed abruptly, grains inside a dense packing exhibit a stepwise descent (under the influence of gravity) [42]. In addition, signs of extraordinary grain motion in response to the reversal of non-uniform shearing have been observed in the surface flow of grains in a Couette geometry [29]. (In Chapter 5, we analyze the response of a granular packing to the reversal of shearing, based on the measurements of internal grain motion and time-resolved volume measurements.) Theoretical works have demonstrated anisotropic texture developed in sheared granular packings [17, 40, 1]. Internal grain motions during the reversal of shearing presumably reflect the readjustment of the anisotropic texture.

Compared to the theory for rapid flows, the theory for quasi-static granular flows is less developed. A number of analytic theories and models involving frictional interaction and plasticity have been attempted [2, 12, 26, 34, 45, 59, 60], while some of the assumed

constitutive relations can be hard to verify on a microscopic level. For these slowly creeping granular particles, the contact forces between densely packed grains dominate the dynamics. Approaches using kinetic theory may be of limited value for these packed grains. For instance, it has been estimated [28] that for millimeter-sized glass beads moving at a relative speed of several bead diameters per second under the static pressure of a layer of material that is several centimeters thick, the mean kinetic energy is actually smaller than the average elastic energy, and may be the least important quantity in accounting for the creeping dynamics. Recent theories show that the elasticity of grains can often play a vital role in the rheology of dense granular flows [7]. It is also known that changing the stress level in a sheared large-scale granular packing can qualitatively alter its velocity profile as a result of differences in the contact network, even though the corresponding fractional deformations of individual grains are all very small [1].

The connection between the internal structure of the material and the rheology of flow is particularly interesting. Here we sample a few previous investigations on shear-induced ordering in systems not limited to granular flows. Shear-induced ordering has been observed in computer simulations of uniformly sheared particle suspensions, in which the fluid-mediated hydrodynamic interactions between particles govern the dynamics [47]—these computations do not impose a thermostat as one might do in other simulations intended for systems of smaller particles with prominent Brownian motions. In computer simulations of particles uniformly sheared under the influence of theoretical thermostats [15, 30, 49, 6, 13], intrinsic time scales controlled by the imposed temperature can be defined, such as the mean diffusion time or thermal collision interval. The observed ordering behavior often depends on the rate of the macroscopic shear. The simulations of sheared particles with repulsive interactions (mimicking the behavior of dilute charged colloidal particles [8]) suggest that the presence of a shear velocity field can either enhance or suppress particle ordering [49, 6]. However, due to the difficulties in connecting these computations to specific experimental conditions, the proper interpretation of the ordering in these simulations with artificial thermostats is apparently still controversial, as is pointed out in Ref. [13]. In experiments of uniformly sheared colloidal suspensions, researchers have demonstrated that particles can exhibit ordering that leads to significant change of rheology, e.g., in Ref. [41, 21].

Note that, for a thick sheared packing, the velocity of grains can extend many orders of magnitude. The characteristic time for local relative displacement between grains, defined by the inverse of the local velocity gradient, exhibits a wide spectrum. Some interesting questions arise: Can a sheared granular packing exhibit spatial order in the presence of such a strong inhomogeneity in space? How does the internal order impact the rheology of granular flow? Experimentalists have observed ordering of granular spheres when grains are poured into vibrating containers with suitable boundary conditions [43, 37]. Recent soft sphere simulations of a large-scale gravity-driven granular flow [48] also find intermittent crystallization on an ordered substrate. However, existing theories of densely packed granular flows [2, 12, 26, 34, 45, 59, 60] generally have not included the effect of spatial order, partly because of the scarcity of experimental information about the internal structure of steadily flowing granular particles.

1.2 Scope of the present work

The goal of the dissertation is to investigate the dynamics of dense granular flow in the quasi-static regime, with special focus on: (1) the time evolution of a shear flow, (2) the connection between internal structure and granular rheology, (3) the development of the bulk properties with the size of the packing, and (4) the factors that determines the spatial distribution of particle velocity. The model system contains glass particles in an annular channel. The granular material is subjected to a fixed vertical load, and is sheared from above at a constant or alternating speed. Simultaneous measurements of internal particle structure, granular volume, and boundary shear force are performed as the granular packing evolves over time. Internal velocity fields and time-resolved trajectories of particles are measured. This system provides information that is complimentary to prior experiments using standard Couette cells, which usually feature a rotating cylinder and a free surface of grains.

We first focus on spherical particles of a nearly uniform size. More generally, polydispersity would introduce another factor affecting the evolution of the packing; a movie demonstrating the shear-induced segregation of a mixture of particles of different sizes in

our system is available on-line. ¹ In the present work, we limit the examples to mono-disperse spherical objects, whose evolution does not involve size segregation, and whose stationary state consequently has a spatially uniform composition. Partial results are published in Ref. [56] and in subsequent papers [53, 54, 52]. The extension to more realistic situations involving poly-dispersity or non-spherical particulates is under way.

Also, we create flow conditions with a hierarchy of forces in which the typical contact force between grains is much larger than the weight of one grain, which is in turn much greater than the maximal drag force provided by interstitial fluid. Therefore, the presence of fluid for imaging purposes in this work does not play a significant role in the quasi-static motions of grains, except by reducing the friction between particles or between particles and stationary walls through lubrication.

1.3 Granular flows in other regimes

A number of papers on granular shear flows in the same geometry as in our work are reported in the literature, but with focus on other aspects and in different dynamical regimes. In addition to the local contact force measurements already cited [32], there are other experiments using low normal load and high shear rates. The relation between shear force and shear rate [19, 46], as well as the granular self diffusion as seen from the sidewall [25], are reported in these experiments focusing on the behaviors in the rapid-flow regime. In addition, some previous works in the same geometry focus on stick-slip behavior [11], whereas we impose a stationary driving in the precision measurement of the internal velocity fields.

Different dynamical regimes can coexist spatially in stationary flows. The high-speed shear flows cited as Refs. [19, 46, 25] are examples in a closed geometry. This spatial inhomogeneity is also commonly seen in experiments on granular flows with a free surface. For instance, in gravity-driven flows with an inclined grain surface [27, 50], distinct behaviors are found for the rapidly flowing particles near the upper surface and the slowly creeping grains deeper in the bulk. The kinematical inhomogeneity of the standard Couette flow can arise from the vertical gradient of compressive stress, which starts from zero at its free

¹http://www.haverford.edu/physics-astro/gollub/internal_imaging

surface and increases downwards. This inhomogeneity becomes increasingly important as the upper regions are agitated by higher shear rates. This situation eventually becomes a complicated 3D problem when the centrifugal force on individual grains are large enough.

The preceding examples do not cover the situation where the dynamical regimes of a granular system alternate over time. The alternation can be induced by an external periodic driving, or, it can be spontaneous in the circumstance that density waves occur [55].

Chapter 2

Experimental Methods

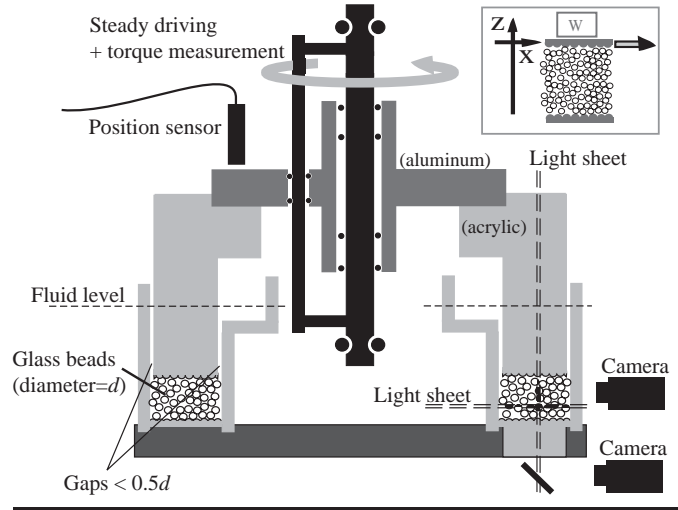


Figure 2.1: Cross-section of the annular channel filled with glass beads, with the inset showing a schematic side view and the definition of coordinates being used in this work. The shear and normal load W are transmitted through a mono-layer of glass beads glued to the rotating aluminum-acrylic assembly that is free to move vertically while maintaining constant rotation rate. Three different bottom conditions are available: flat, mono-layer and bumpy. Volume change is determined by detecting the vertical displacement of the upper assembly. The torque required to maintain the rotation is measured by a force gauge coupled to the motor through a pulling wire (not shown). Both vertical and horizontal slices of internal fluorescent images can be captured by digital cameras.

2.1 Main apparatus

The main apparatus is an annular channel formed by two concentric stationary glass cylinders, which are smooth and transparent (Fig. 1). We typically use spherical soda lime glass beads (density $\approx 2.5\text{g/cm}^3$, elastic modulus $\approx 63\text{ GPa}$, refractive index ≈ 1.54 , from Jaygo Inc.) of mean diameter $d = 0.68\text{mm}$ with a standard deviation 4% to fill the channel; the filling height is adjustable from a few particle diameters to $50d$. The distance between the inner and the outer walls is about $28.5d$ and the circumference is about $800d$. Fluid can be added to the inter-particle space when internal imaging (described below) is planned. The glass beads are driven by a rotating ring-shaped upper boundary to which a mono-layer of glass beads has been glued; the glued glass beads are packed at about the maximal area density and form local hexagonal structures with dislocations. Three

different bottom boundary conditions are available: (1) flat bottom - smooth acrylic; (2) mono-layer bottom (described above); and (3) bumpy bottom - a mixture of 0.6mm and 1.0mm glass beads glued at approximately equal area fraction. In addition, a transparent window (thick polycarbonate) is made at the bottom of one part of the channel. The top surface of the acrylic part of the rotating assembly is also polished, to provide an option for viewing from the top.

The upper boundary is attached to a precision bearing that allows free but strictly vertical movement while rotating. The weight of the upper boundary assembly W provides a constant normal load of $(1.3\text{Kg})g$, which is about 12 times the total effective weight of the (fluid-immersed) grains at the typical filling height of $24d$. Extra precision is demanded during the assembly process to ensure that the two planes defined by the upper and lower boundaries are parallel, and that the gaps between the upper boundary and the cylindrical walls are smaller than $0.5d$ around the circumference at all times, while the upper boundary rotates. The small gaps, combined with a fluid reservoir at the upper edge of the inner wall, allow the interstitial gas or fluid to exit or re-enter the channel freely, while the granular particles cannot escape. This allows the determination of the granular volume change by monitoring the height of the upper assembly. In practice, the height is measured once per rotation by detecting the position of a horizontal metallic arm installed on the rotating assembly and extending beyond the outer radius of the channel. An inductive-capacitive sensor is used for this purpose. (The design of the extended arm enables us to avoid calibration errors when the sensor is displaced, e.g., when changing particles.)

The unidirectional rotation is driven by a stepping motor (DM-4001 by Aerotech Inc.) whose rotating shaft is rigidly connected to and aligned with the central shaft of our apparatus; the central shaft rotates with the same angular speed of the upper boundary, as shown on the figure. The combination of the micro-stepping of the motor and a 100X speed reduction gear box gives an angular resolution of 2.5×10^{-5} rotations. Extra care is taken to maximize the rigidity of the driving mechanism. The deviation of motion of the upper boundary from an ideal constant-speed translation is less than $0.1d$; this is estimated by monitoring the projection (onto a distant screen) of a laser beam reflected from a mirror installed on the central shaft of our apparatus.

The shear force at the upper boundary can be determined if one measures the torque

transmitted from the motor to the upper boundary or, alternatively, the torque that is required to resist the motor’s tendency to rotate in the opposite direction. This is achieved by letting the motor stand freely on its own rotating shaft, decoupling it from its usual rigid support, attaching a pulling wire off center, and measuring the tension in the wire with a force gauge (PCB Piezotronics: KT-1102-01). However, the flexibility introduced by the pulling wire inevitably causes some unsteadiness in the upper boundary motion, so the motor is rigidly supported when the velocity profile is measured.

2.2 Internal imaging and image analysis

To image the interior, the inter-particle space is filled with a special hydrocarbon mixture (viscosity $\approx 10\text{cS}$, density $\approx 1\text{g/cc.}$, from Cargille Laboratories.). The refractive index of the fluid is fine-tuned to match that of the beads by adjusting the relative concentration of the ingredients to the accuracy of 10^{-3} . The optimal index-matching condition is determined by minimizing the scattering near the forward direction while a green He-Ne laser beam (543.5nm) is sent through a test cell containing the the mixture of beads and fluid. In gluing beads to the upper or lower boundary, adhesive (Norland NOA-68) with the closest refractive index to that of the glass beads is chosen and bubbles are avoided, in order to minimize the distortion of the image or the illuminating light sheet (described below) through these roughened boundaries.

A minimal amount of fluorescent dye (Exton Pyrromethene-580, fluorescent peak $\approx 540\text{nm}$) is blended into the fluid. A thin laser sheet enters the imaging region through either the bottom window or the front wall, to activate the fluorescence of the dye and create an instantaneous 2D image slice $\mathcal{I}_{slice}(\vec{x}, t)$ in which particles appear as shadows. The image can be captured by digital camera through either the front wall or the bottom window. To create the laser sheet, a narrow beam from the 514.5nm line of an argon ion laser (Lexel-75) is first expanded isotropically (by a microscope objective), then collimated (by a convex lens), and finally compressed one-dimensionally by a set of cylindrical lenses. (For this purpose, we use a pair of convex and concave lenses to create a tunable effective focal length $f \sim 2\text{m}$, and a convex lens with $f = -6\text{mm}$, located between the focal point of the tunable lens pair and our imaging area.) The resulting laser sheet is narrower than

$0.5d$ throughout the region of interest. The fluorescent images are filtered with a cut-off wave-length 550nm before reaching the camera, to screen out the undesired noise due to scattering of the excitation light.

To track the particles, an image is first converted to a 2D map \mathcal{M} using a convolution

$$\mathcal{M}(\vec{x}, t) = \int G'(|\vec{x} - \vec{x}'|) \cdot \mathcal{I}_{slice}(\vec{x}', t) \cdot d^2\vec{x}' \quad (2.1)$$

in which $G'(r)$ stands for the derivative of a gaussian ring

$$G'(r) = \frac{d}{dr} e^{-(r-a_0)^2/2\sigma_0^2} \quad (2.2)$$

with radius a_0 being approximately the apparent radius of a particle in the image (from 9 to a few tens of pixels, depending on the image magnification), and the width σ being one or a few pixels. In practice, the convolution takes advantage of FFT techniques for the sake of computational efficiency [44]. The bright peaks in each map \mathcal{M} represent the centers of particles in that frame, and are found using previously developed computer routines [10] which also reconstruct particle trajectories from a set of sequential images. This convolution method is based on the idea of edge recognition (similar to Hough transformation [3]), and therefore can still resolve particles in the presence of certain degree of particle overlap (due to the finite thickness of the light sheet). When high precision measurement of instantaneous individual particle positions (as opposed to coarse-grained mean velocity measurement) is needed, the light sheet is set to be as narrow as possible, and a high threshold of the peak intensity is selected so that only very sharp peaks (contributed by particles whose centers are precisely on the symmetrical plane of the light sheet) are admitted as valid data. The ultimate limit of precision in determining particle positions is set by the pixel width, corresponding to a few tenths of a particle diameter (depending on magnification.) All computations are performed using IDL programming. Images demonstrating the quality of the particle recognition are included in Appendix B.1.1.

We also analyze the spatial spectrum of each image slice. For instance, the horizontal spatial periodicity of a vertical image slice $\mathcal{I}_{slice}(x, z, t)$ can be represented by the following normalized Fourier spectrum averaged over depth z

$$f(k_x, t) = \left\langle \frac{|F(k_x, z, t)|}{(\int |F(k_x, z, t)|^2 dk_x)^{\frac{1}{2}}} \right\rangle_z \quad (2.3)$$

in which $F(k_x, z, t) = \mathcal{F}_x[\mathcal{I}_{slice}(x, z, t)]$ stands for the Fourier transform in the x direction. The denominator is to correct the variation of image intensity over z and t . The intensity of a peak of this normalized spectrum $f(k_x, t)$ at a particular wave number $k_x^{(1)}$, corrected by subtraction of the background value, is defined as

$$I^{(1)}(t) = \frac{1}{2\epsilon} \int_{k_x^{(1)} - \epsilon}^{k_x^{(1)} + \epsilon} |f(k_x, t)|^2 dk_x - I_B^{(1)}(t) \quad (2.4)$$

where $I_B^{(1)}(t)$ is a background value determined by averaging $|f|^2$ over a broader spectral interval centered at $k^{(1)}$ but excluding the wave-numbers within $(k_x^{(1)} \pm \epsilon)$. When the wave-number $k_x^{(1)}$ is chosen to match the mean horizontal spacing ($\approx 1d$) of particle centers in the crystallized state, the calculated peak intensity $I^{(1)}(t)$ can be used as an indicator of the growth of the crystalline order.